Supporting Information

for

Facile synthesis and bonding of 4-ferrocenyl-1,2,4-triazol-5-ylidene complexes

Michal Franc, Jiří Schulz and Petr Štěpnička*

Department of Inorganic Chemistry, Faculty of Science, Charles University,

Hlavova 2030, 128 40 Prague, Czech Republic

E-mail address: stepnic@natur.cuni.cz

Contents

Synthesis of 1 and 2

Preparation of 4-ferrocenyl-4*H*-1,2,4-triazole (1). Solid aminoferrocene (100.5 mg, 0.50 mmol) was added to a solution of *N*,*N*′-bis(dimethylaminomethylene)hydrazine (72.6 mg, 0.50 mmol) in dry toluene (8 mL), followed by *p*-toluenesulfonic acid monohydrate (≈5 mg), and the resulting mixture was heated at gentle reflux under nitrogen for 3.5 h, whereupon its colour changed from orange to dark red. Next, the mixture was concentrated under vacuum and the dark residue was purified by chromatography over a silica gel column. Initially, cyclohexane-ethyl acetate (1:1) was used to remove unreacted aminoferrocene (approximately 25 mg of the amine was recovered). Subsequent elution with dichloromethane-methanol (10:1) developed a yellow band due to the cyclization product, which was collected and evaporated leaving triazole **1** as a yellow solid. Yield: 88.6 mg (70%).

^{1}H NMR (400 MHz, $CDCl_3$): δ 4.26 (s, 5H, C_5H_5), 4.28 (t, *J*′ = 2.0 Hz, 2H, C_5H_4), 4.56 (t, *J*′ = 2.0 Hz, 2H, C_5H_4), 8.36 (s, 2H, NCH). ^{13}C{^{1}H} NMR (151 MHz, $CDCl_3$): δ 63.01 (s, CH of C_5H_4), 66.85 (s, CH of C_5H_4), 70.05 (s, C_5H_5), 90.50 (s, C^{ipso}-N of C_5H_4), 143.00 (s, NCH). ESI+ MS: *m/z* 254 ([M + H]$^+$). The analytical data matched those in the literature.[1]

Synthesis of 2. Neat iodomethane (0.93 mL, 150 mmol; 30 equiv.) was introduced to a solution of triazole **1** (126.5 mg, 0.50 mmol) in dry dichloromethane (10 mL), and the mixture was stirred at room temperature in the dark for 6 h (some precipitate formed during this time). Then, the mixture was concentrated under reduced pressure and the yellow solid residue was purified by chromatography over a silica gel column, eluting with dichloromethane-methanol (20:1). A single yellow band was collected and evaporated to produce salt **2** as a yellow microcrystalline solid. Yield of **2**·1/6CH_2Cl_2: 180 mg (88%). Note: the compound partly decomposes upon prolonged storage (several months) under ambient conditions.

^{1}H NMR (400 MHz, CD_2Cl_2-CD_3OD 5:1): δ 4.36 (s, 3H, CH_3), 4.40 (s, 5H, C_5H_5), 4.40 (t, *J*′ = 2.0 Hz, 2H, C_5H_4), 4.97 (t, *J*′ = 1.9 Hz, 2H, C_5H_4), 8.50 (s, 1H, NCH), 11.58 (s, 1H, NCH). ^{13}C{^{1}H} NMR (151 MHz, CD_2Cl_2-CD_3OD 5:1): δ 41.98 (s, CH_3), 65.41 (s, CH of C_5H_4), 70.24 (s, CH of C_5H_4), 73.02 (s, C_5H_5), 89.32 (C^{ipso} of C_5H_4), 142.27 (s, NCH), 142.32 (s, NCH). ESI+ MS: *m/z* 268 ([M – I]$^+$). The analytical data agreed with those reported in the literature.[2]

X-ray crystallography

Full-sphere diffraction data ($\pm h \pm k \pm l$, $2\theta_{max}$ = 55°) were collected with a Bruker D8 VENTURE Kappa Duo diffractometer equipped with a Cryostream Cooler (Oxford Cryosystems) using Mo Kα radiation (λ = 0.71073 Å). The structures were solved by direct methods (SHELXT-2018[3]) and subsequently refined using a least-squares routine based on F^2 (SHELXL-2017[4]). All nonhydrogen atoms were refined with anisotropic displacement parameters. Hydrogen atoms at the η^2-coordinated double bonds and the disordered methyl substituent in the structure of compound **3** were identified on a difference electron density map and refined as "riding atoms" with U_{iso}(H) set to multiple of U_{eq} of the bonding carbon atom. Other hydrogen atoms were included in their theoretical positions and refined similarly using the standard parameters implemented in SHELXL.

Selected crystallographic data and structure refinement parameters are presented in Table S1. All geometric data and structural diagrams were obtained using a recent version of the PLATON program.[5] The numerical values were rounded with respect to their standard deviations.

Table S1. Selected crystallographic data and structure refinement parameters

Compound	**3**	**4**·$CHCl_3$
Formula	$C_{21}H_{25}FeIN_3Rh$	$C_{41}H_{50}AuCl_3FeIN_5$
M	605.10	1098.92
Crystal system	monoclinic	monoclinic
Space group	$P2_1/c$ (no. 14)	Cc (no. 9)[c]
T [K]	120(2)	120(2)
a [Å]	12.0867(3)	20.2983(6)
b [Å]	13.1442(3)	14.2658(4)
c [Å]	13.3802(3)	15.5783(4)
α [°]	90	90
β [°]	104.694(1)	108.205(1)
γ [°]	90	90
V [Å]^3	2056.19(8)	4285.2(2)
Z	4	4
F(000)	1184	2160
μ(Mo Kα) [mm^{-1}]	3.020	4.700
Diffrns collected	17730	55568
Independent diffrns	4730	9783
Observed diffrns[a]	4396	9762
R_{int}[b] [%]	1.93	2.78
No. of parameters	244	478
R[b] obsd diffrns [%]	1.66	1.84
R, wR[b] all data [%]	1.92, 3.48	1.84, 4.65
Δρ [e Å^{-3}]	0.42, −0.59	0.75, −1.39
CCDC deposition no.	2345618	2345619

[a] Diffractions with $I > 2\sigma(I)$. [b] Definitions: $R_{int} = \Sigma \left| F_o^2 - F_o^2(\text{mean}) \right| / \Sigma F_o^2$, where F_o^2(mean) is the average intensity of symmetry-equivalent diffractions. $R = \Sigma \left| \left| F_o \right| - \left| F_c \right| \right| / \Sigma \left| F_o \right|$, w$R$ = $[\Sigma\{w(F_o^2 - F_c^2)^2\}/\Sigma w(F_o^2)^2]^{1/2}$. [c] Flack's enantiomorph parameter: 0.000(2).

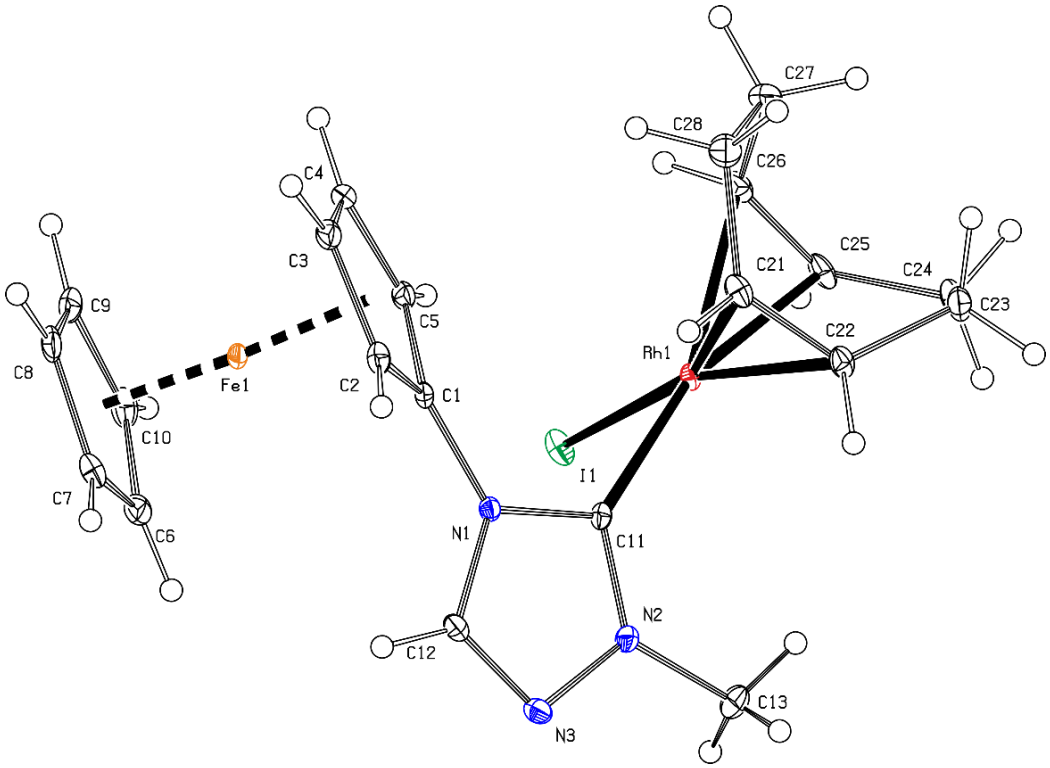

Figure S1 PLATON plot of the structure of **3** with displacement ellipsoids at the 30% probability level. For clarity, only one orientation of the H atoms at the disordered methyl group is shown.

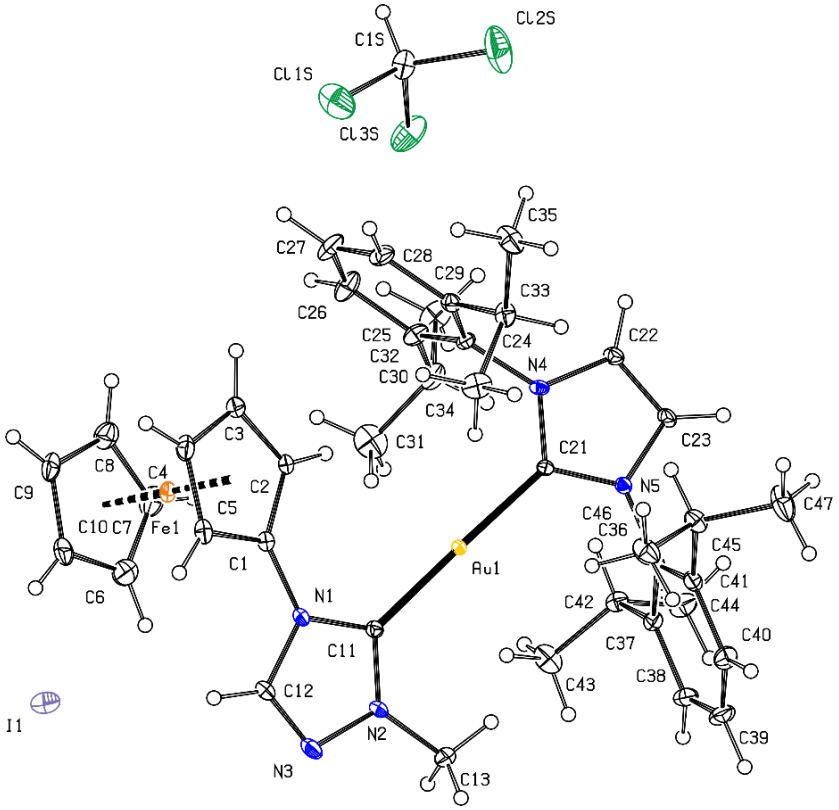

Figure S2 PLATON plot of the structure of **4**·$CHCl_3$ showing displacement ellipsoids at the 30% probability level

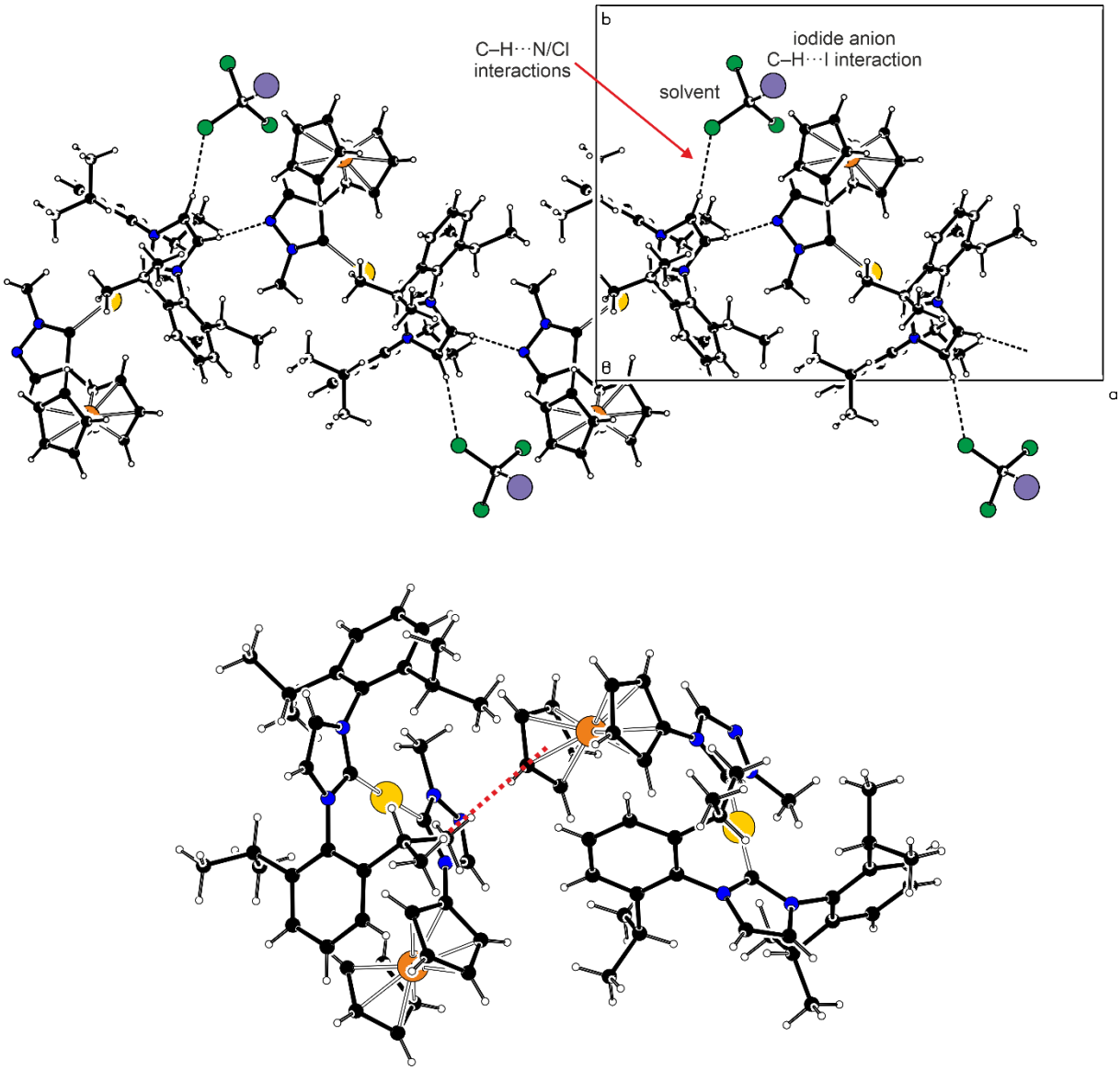

Figure S3 (top) C–H···X (X = N, Cl, and I) hydrogen bonds (projection along the crystallographic *c* axis) and (bottom) π···π interactions in the crystal structure of **4**·$CHCl_3$ (the distance between the ring centroids is 3.823(3) Å and the interplanar angle is 13.8(3)°)

Electrochemical behaviour of triazole 1

Triazole **1** displays a standard reversible oxidation attributable to the ferrocene/ferrocenium redox transition at 0.26 V *vs*. the ferrocene reference (Figure S4). However, when the scan range is extended towards more positive potentials, the anodic wave takes the shape of a stripping peak, which suggests that the oxidized species remains absorbed on the electrode surface.

DFT calculations (Figure S5) showed that the highest occupied molecular orbital (HOMO) of **1** is localised predominantly at the ferrocene unit and composed mostly of the iron 3d orbitals (≈84%) with a contribution from the carbon atoms of the cyclopentadienyl rings (≈11% of 2p(C)). The lowest unoccupied molecular orbital (LUMO) is also centred on the ferrocene (≈42% of 3d(Fe), and ≈39% of 2p(C)), although it partly extends to the triazole substituent (≈18%, $2p_z$(C/N)). More importantly, the change in electron density on going from **1** to $\mathbf{1}^+$, visualised as $\rho(\mathbf{1}) - \rho(\mathbf{1}^+)$ at the geometry of the native species **1**, occurred practically exclusively at the ferrocene unit (Figure S6), which supported the assignment of the redox process to reversible oxidation of the ferrocene group.

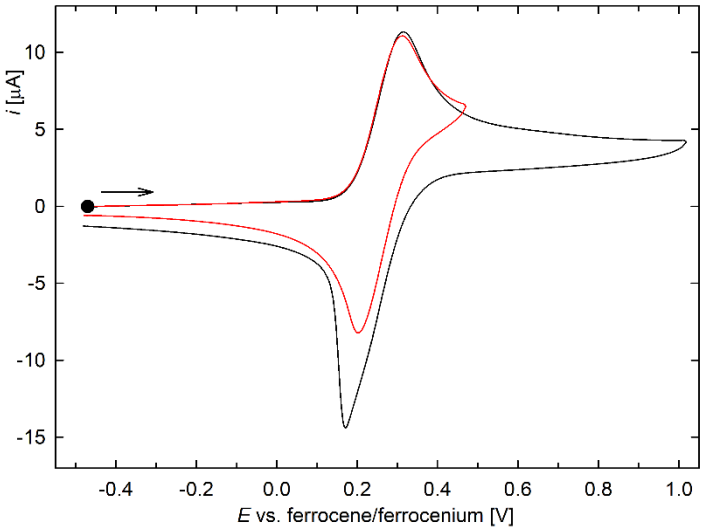

Figure S4 Cyclic voltammograms of triazole **1** (glassy carbon disc electrode, dichloromethane containing 0.1 M $[Bu_4N][PF_6]$, scan rate 100 mV s^{-1}). Voltammograms recorded over different potential ranges are distinguished by different colours.

HOMO LUMO

Figure S5 Frontier molecular orbitals of **1** (contour maps with isosurfaces at ±0.05 a.u.) at the PBE0(d3)/def2-TZVP level of theory (for computational details, see below)

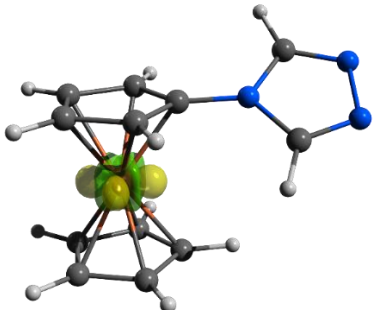

Figure S6 Electron difference map for the oxidation of **1**, ρ(**1**) – ρ(**1**$^{+}$), mapped at the geometry of the native species **1** (isosurfaces at ±0.02 a.u.)

DFT computations

Theoretical calculations were performed using the Gaussian 16 program package.[6] The geometry optimizations were started from atomic coordinates determined by X-ray diffraction analysis, using PBE0[7] density functional in conjunction with the Stuttgart effective core potential[8] used for heavy atoms (Rh, Au, I) and the def2-TZVP[9] basis set for the remaining elements (C, H, N and Fe) with added Grimme's D3 dispersion correction.[10] Orbital composition analysis based on the Natural Atomic Orbitals (NAO)[11] (at the PBE0(d3)/def2-TZVP level of theory) was performed using the Multiwfn software package (version 3.8).[12] Molecular orbitals were visualized using the Avogadro programme.[13] Intrinsic bond orbital (IBO) analysis and visualization of the orbitals were performed using the IboView software.[14]

The frontier molecular orbitals (FMOs) of rhodium complex **3** (Figure S7) were localised mainly at the Rh(cod)I fragment, with only a minor contribution from the carbene ligand and 3d(Fe) orbitals (<3%). In particular, the HOMO was a nonbonding combination of rhodium 4d and 5s orbitals (≈50% 4d(Rh) + ≈3% 5s(Rh)) and an iodine lone electron pair (≈35% I(5p)), while the LUMO corresponded to an overlap of vacant rhodium orbitals (≈18% 5p + ≈10% o 4d) with π* antibonding orbitals of the cod ligand (total ≈47% of 2p(C)). Conversely, the HOMO of **4** (Figure S7) was localised entirely at the ferrocene unit (≈87% 3d(Fe), and ≈12% 2p(C)), and the LUMO was evenly distributed between the two carbene ligands and contributed predominantly from the $2p_z$ orbitals of the donor carbon atoms (≈24% $2p_z(C^{triaz})$, ≈18% $2p_z(C^{IPr})$) and their adjacent nitrogen atoms (≈14% $2p_z(N^{triaz})$, ≈11% $2p_z(N^{IPr})$), with contributions from the metals (≈15% 6p(Au), ≈1% 3d(Fe)).

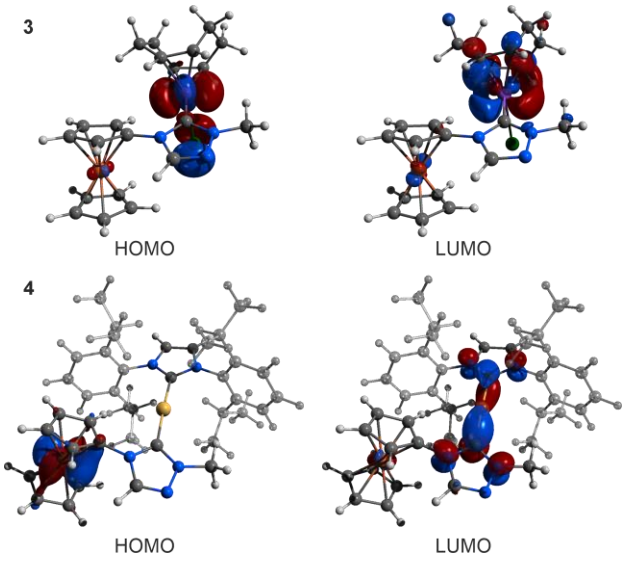

Figure S7 Frontier molecular orbitals of **3** (top) and **4** (bottom; only the complex cation is shown for clarity), depicted as contour maps with isosurfaces at ±0.05 a.u. calculated at the PBE0(d3)/def2-TZVP:sdd(Rh,I,Au) level of theory

Results from IBO analysis

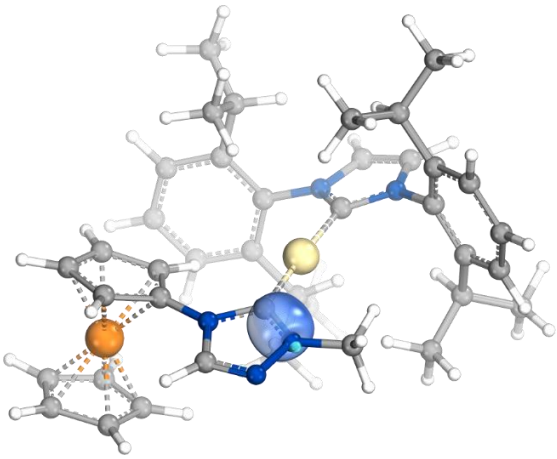

σ(N–C) [1.17(N2)/0.82(C11)]

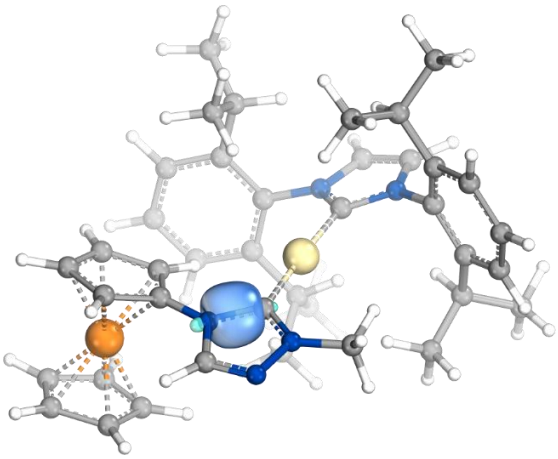

σ(N–C) [1.18(N1)/0.80(C11)]

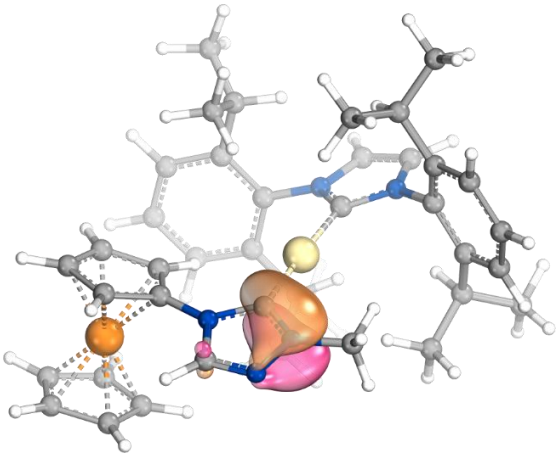

π(N–C)
[1.42(N2)/0.43(C11)/0.05(C12)/0.07(N3)]

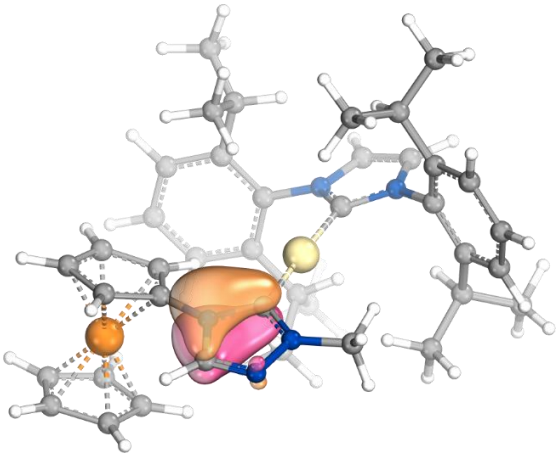

π(N–C)
[1.44(N1)/0.31(C11)/0.16(C12)/0.04(N2)/0.02(C1)]

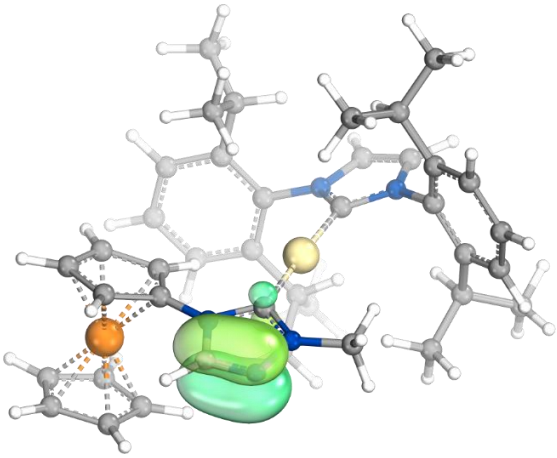

π(N–C) [1.10(N3)/0.79(C12)/0.09(C11)]

Figure S8 Selected intrinsic bond orbitals (IBOs) of **4** illustrating the bonding situation in the *triazolylidene* ligand. Values in parentheses indicate the fraction of bonding electrons assigned to the individual atoms. Atom numbering corresponds with that used for the crystal structures.

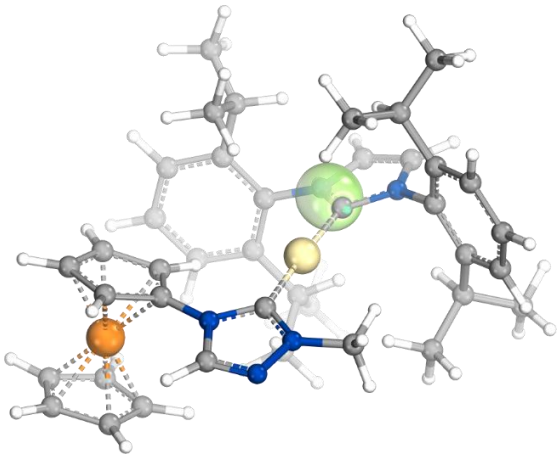

σ(N–C) [1.17(N4)/0.81(C21)]

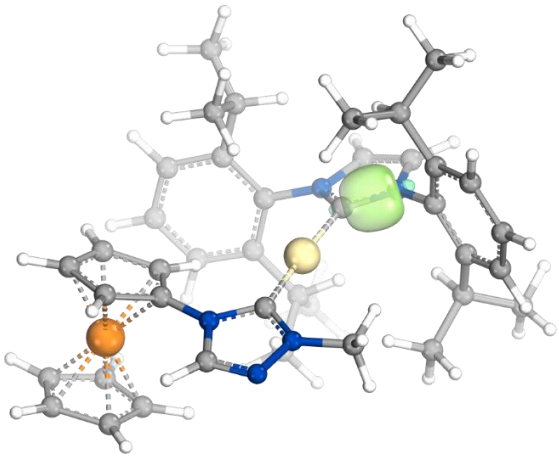

σ(N–C) [1.17(N5)/0.81(C21)]

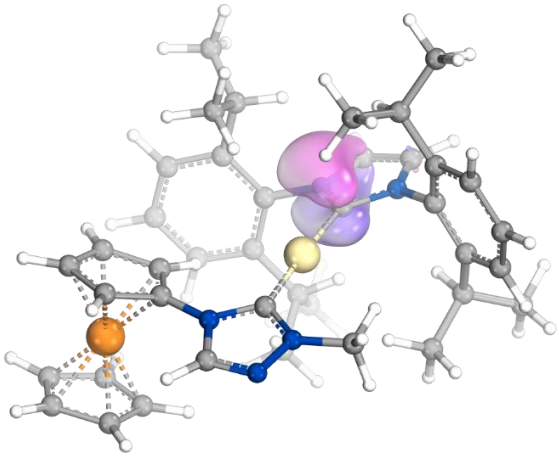

π(N–C) [1.44(N4)/0.37(C21)/0.11(C22)/0.04(C23)]

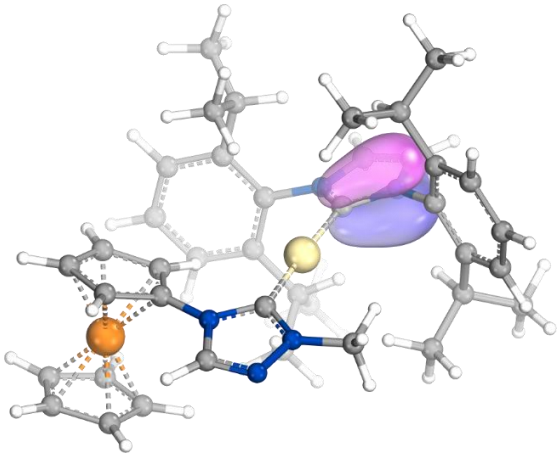

π(N–C) [1.44(N5)/0.37(C21)/0.11(C23)/0.04(C22)]

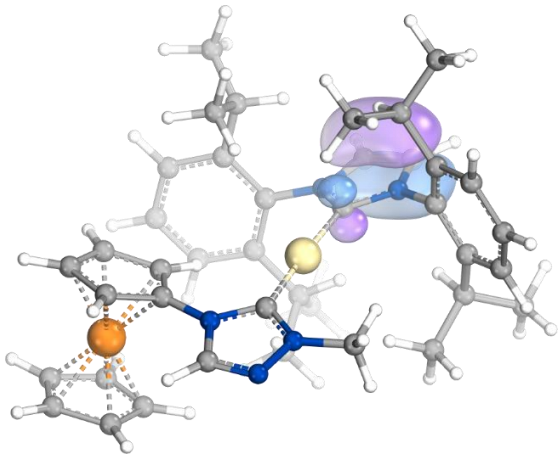

π(C–C) [0.93(C22)/0.93(C23)/0.12(C21)]

Figure S9 Selected intrinsic bond orbitals (IBOs) of **4** for the *imidazolylidene* ligand (IPr). Values in parentheses indicate the fraction of bonding electrons assigned to the individual atoms.

Copies of the NMR spectra

(Note: solvent signals in the NMR spectra are marked with an asterisk.)

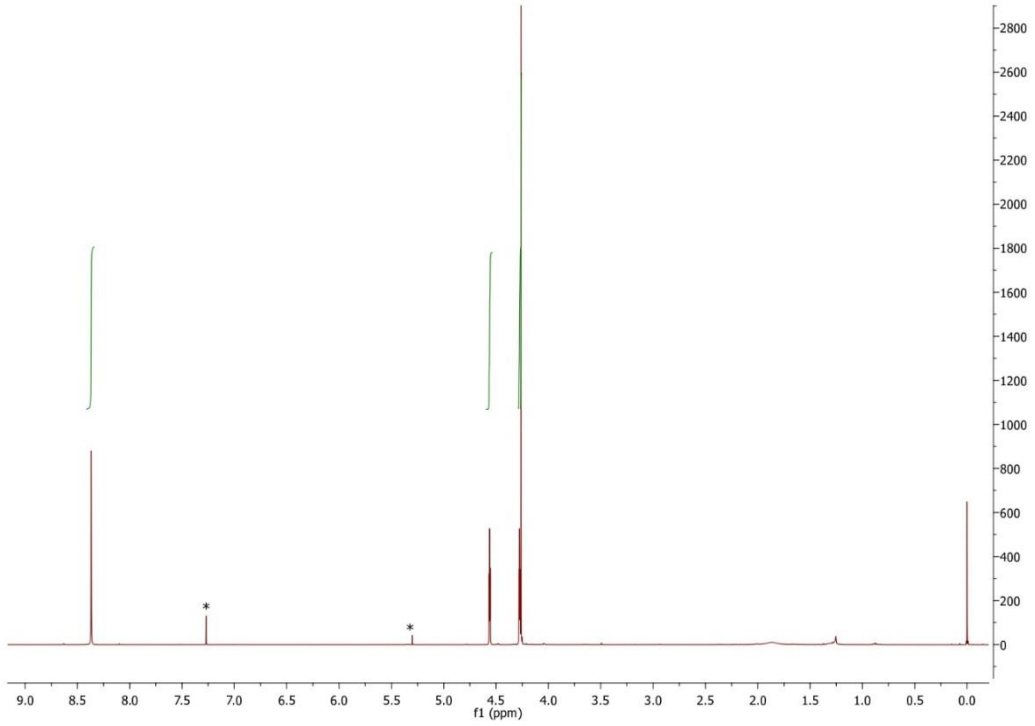

Figure S10 ^{1}H NMR (400 MHz, $CDCl_3$) spectrum of **1**

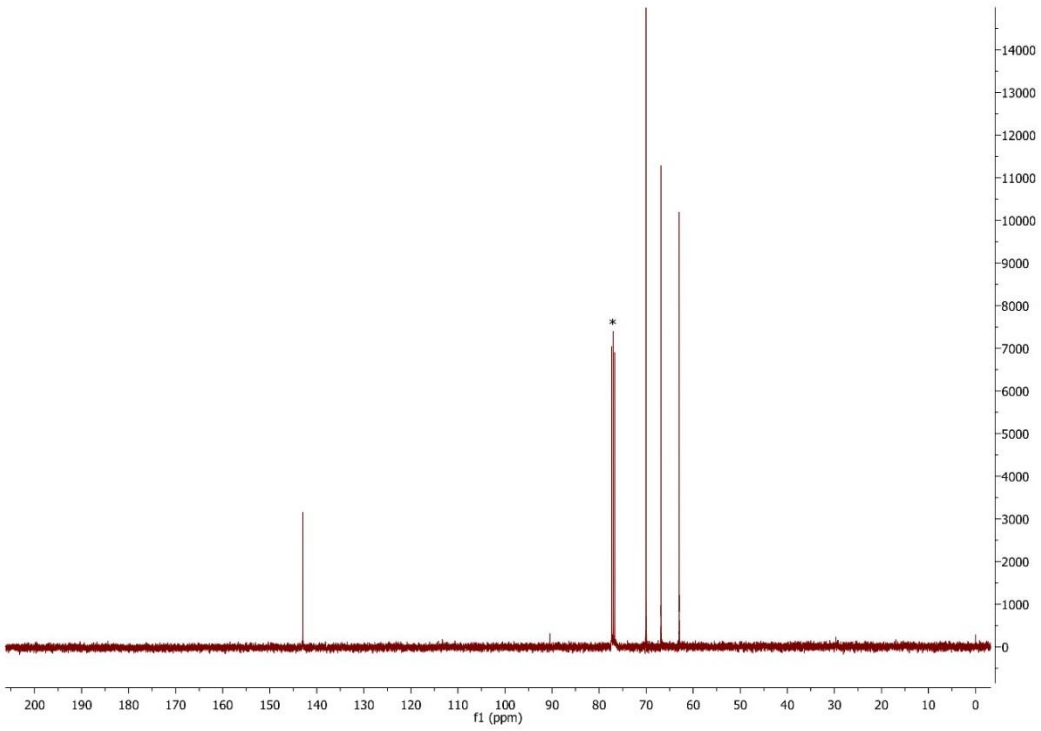

Figure S11 ^{13}C NMR (400 MHz, $CDCl_3$) spectrum of **1**

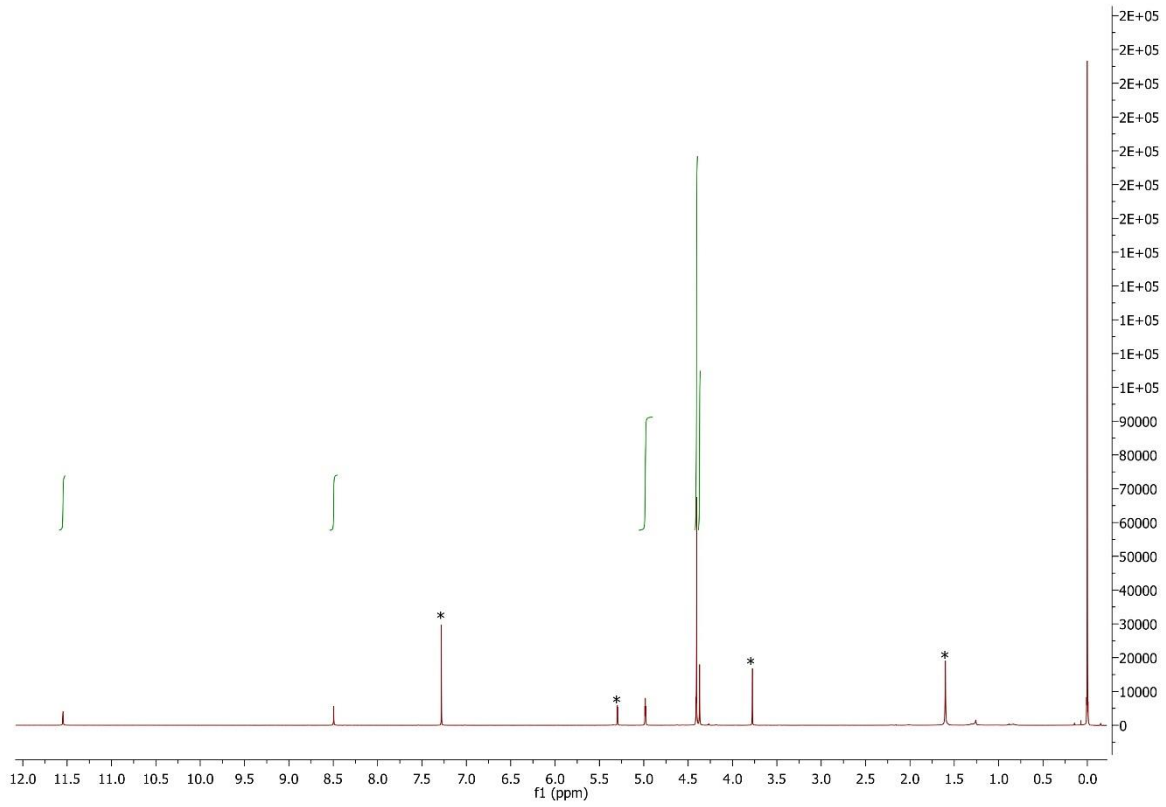

Figure S12 ^{1}H NMR (400 MHz, $CDCl_3$–CD_3OD 5:1) spectrum of **2**

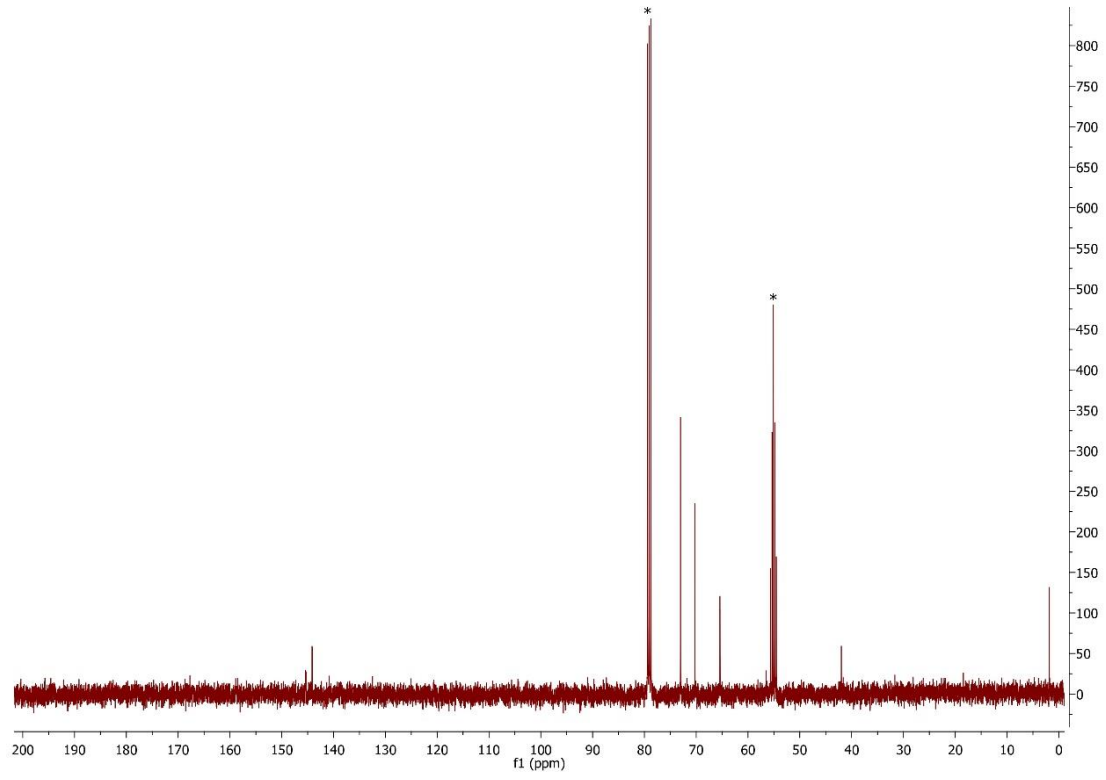

Figure S13 ^{13}C NMR (400 MHz, $CDCl_3$–CD_3OD 5:1) spectrum of **2**

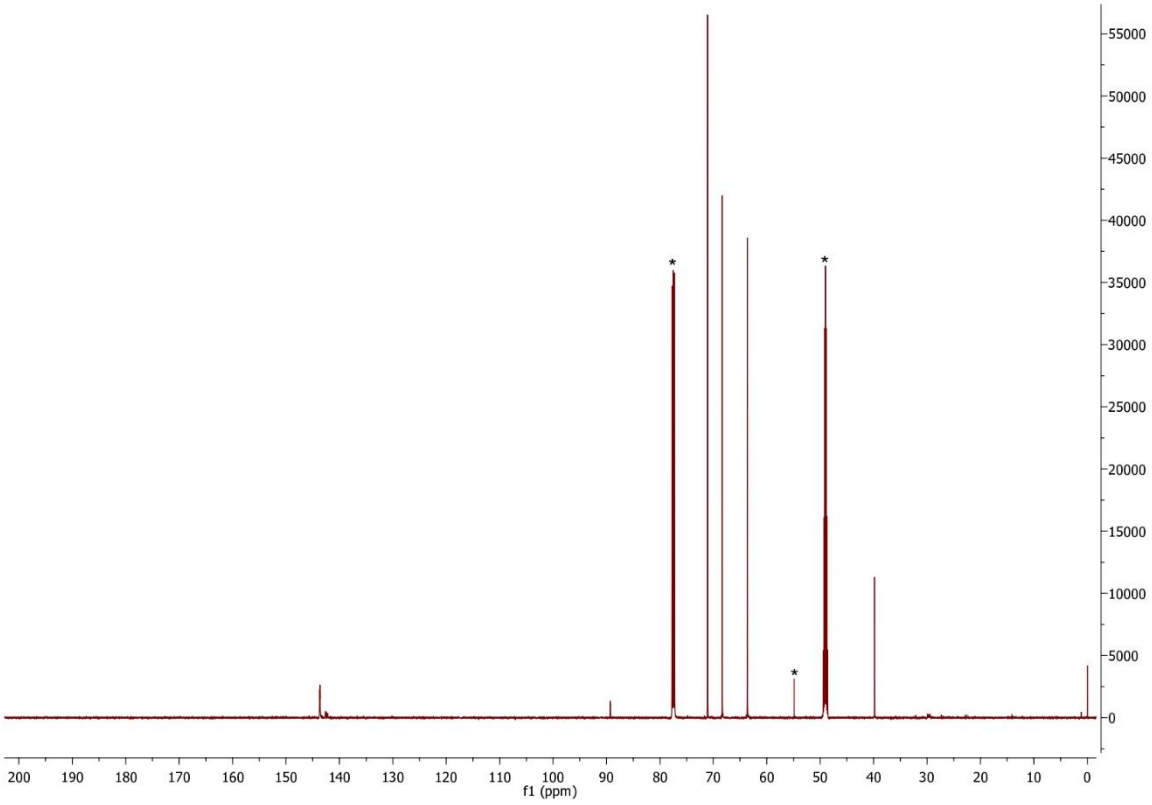

Figure S14 ^{13}C NMR (400 MHz, $CDCl_3$–CD_3OD 2:1) spectrum of **2**

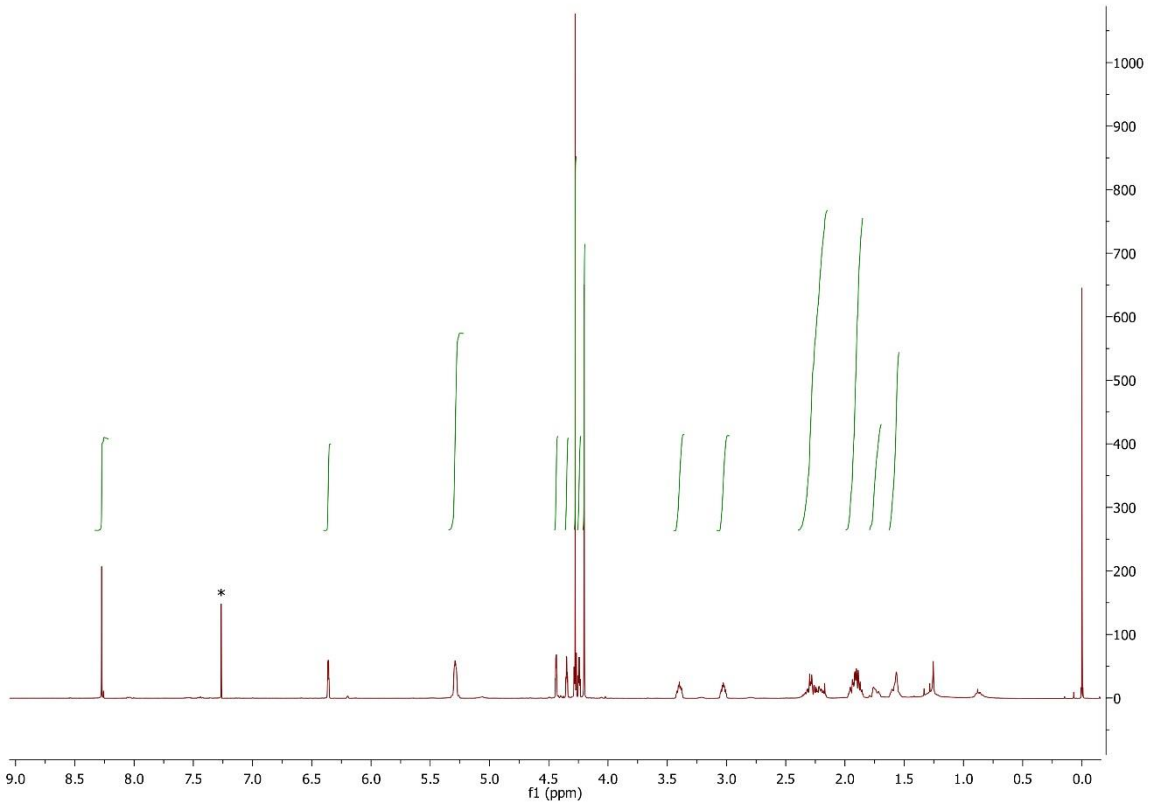

Figure S15 ^{1}H NMR (400 MHz, $CDCl_3$) spectrum of **3**

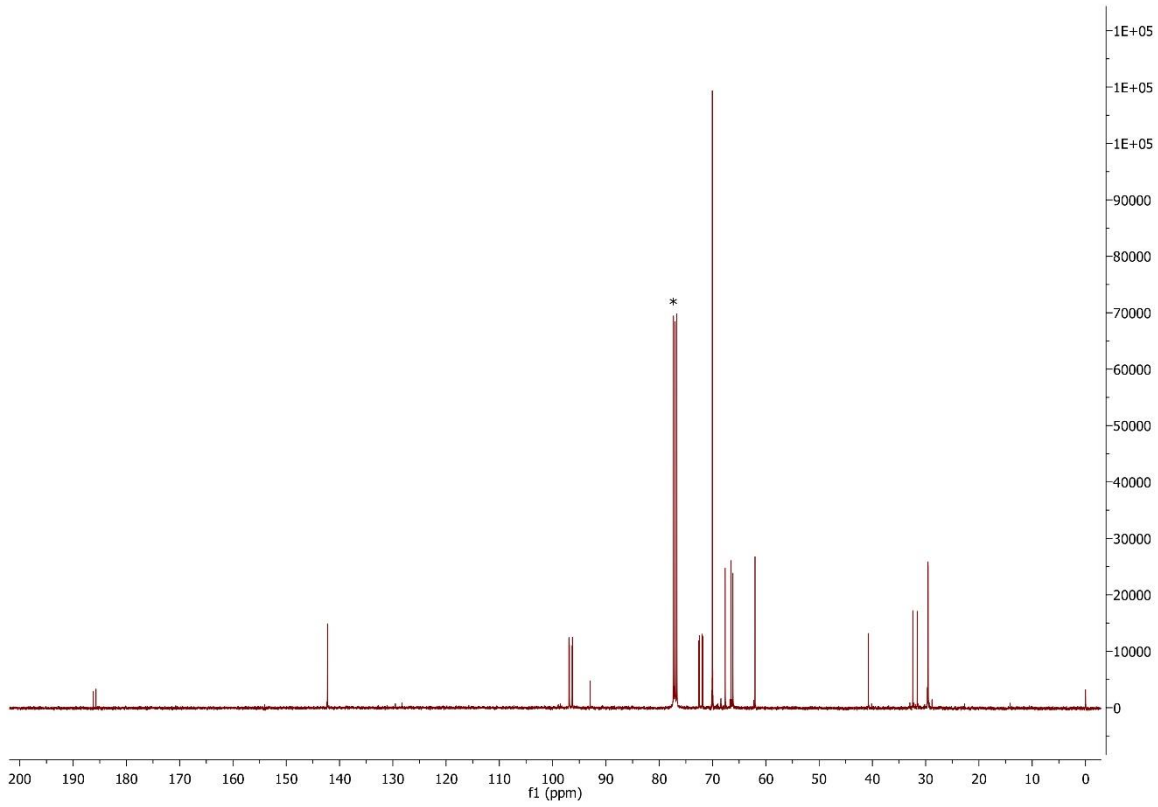

Figure S16 ^{13}C NMR (400 MHz, $CDCl_3$) spectrum of **3**

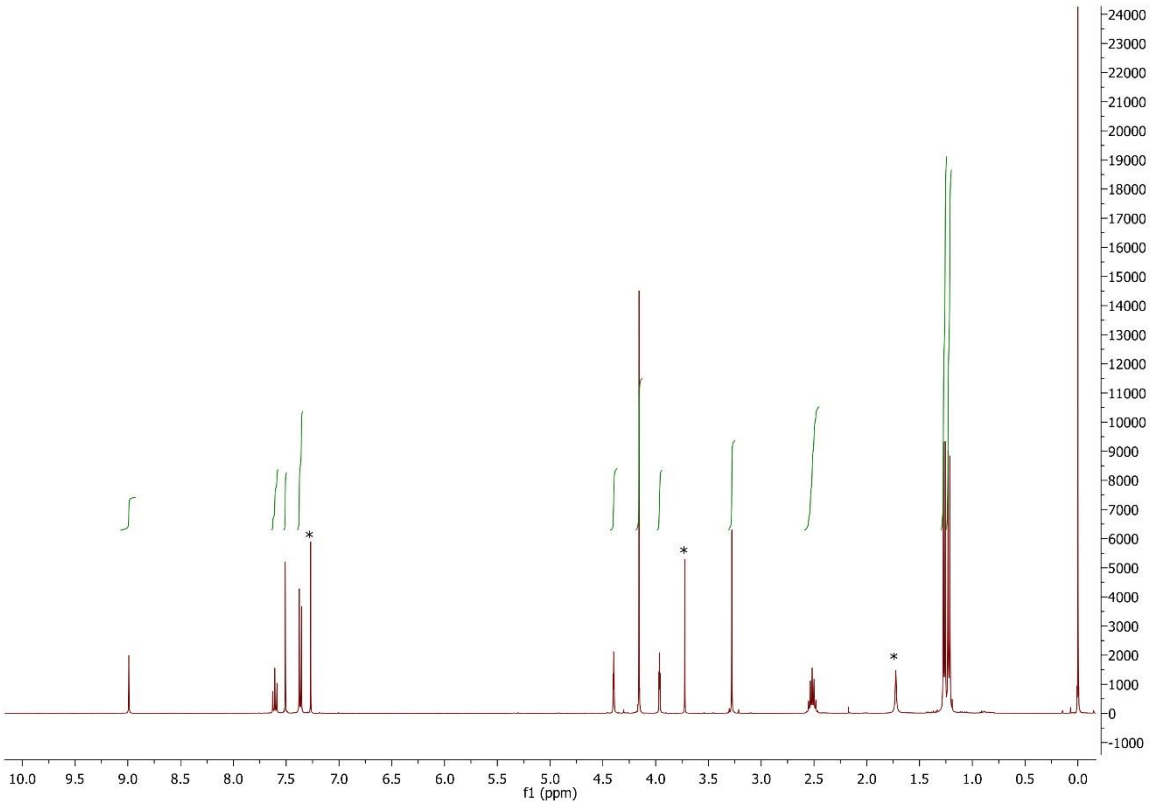

Figure S17 ^{1}H NMR (400 MHz, $CDCl_3$) spectrum of **4**

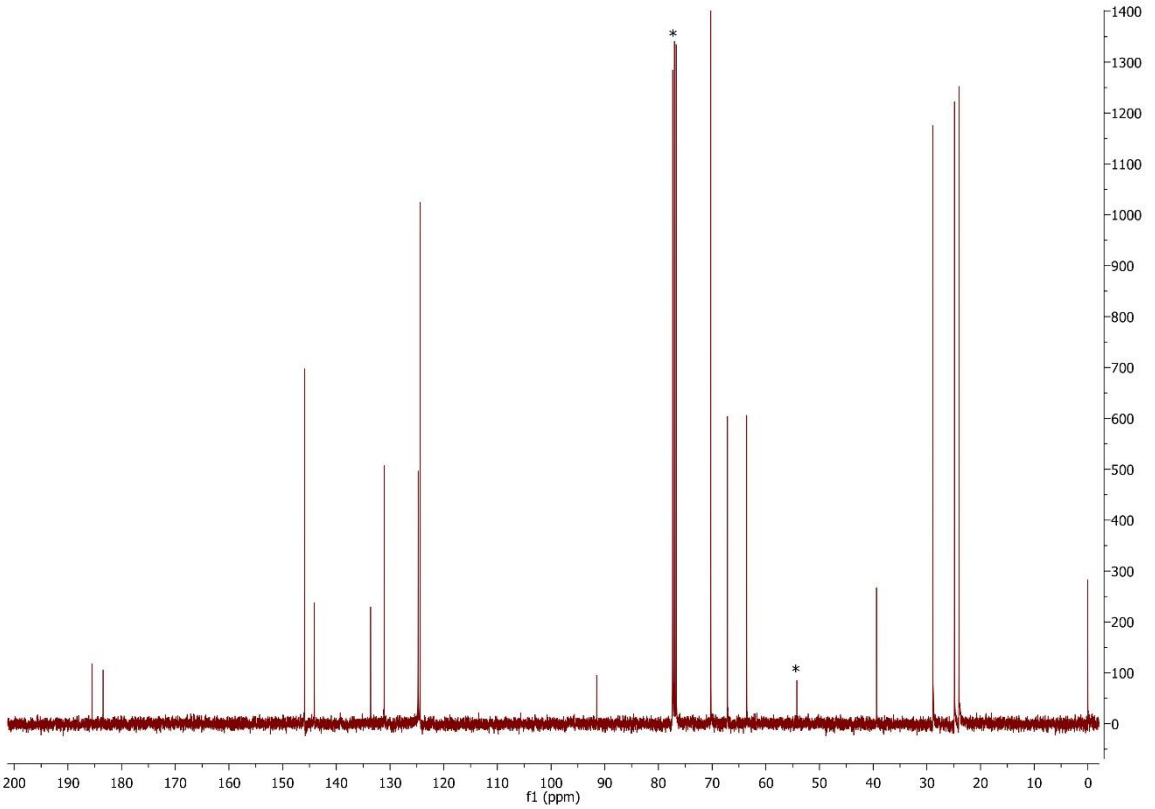

Figure S18 ^{13}C NMR (400 MHz, $CDCl_3$) spectrum of **4**

References

1 T. Mochida, H. Shimizu, S. Suzuki and T. Akasaka, *J. Organomet. Chem.*, 2006, **691**, 4882.

2 Y. Miura, F. Shimizu and T. Mochida, *Inorg. Chem*., 2010, **49**, 10032.

3 G. M. Sheldrick, *Acta Crystallogr., Sect. A: Found. Adv.*, 2015, **71**, 3.

4 G. M. Sheldrick, *Acta Crystallogr., Sect. C: Struct. Chem*., 2015, **71**, 3.

5 a) A. L. Spek, *J. Appl. Crystallogr*., 2003, **36**, 7; b) A. L. Spek, *Acta Crystallogr. D, Biol. Crystallogr*., 2009, **65**, 148.

6 M. J. Frisch, G. W. Trucks, H. B. Schlegel, G. E. Scuseria, M. A. Robb, J. R. Cheeseman, G. Scalmani, V. Barone, G. A. Petersson, H. Nakatsuji, X. Li, M. Caricato, A. V. Marenich, J. Bloino, B. G. Janesko, R. Gomperts, B. Mennucci, H. P. Hratchian, J. V. Ortiz, A. F. Izmaylov, J. L. Sonnenberg, D. Williams-Young, F. Ding, F. Lipparini, F. Egidi, J. Goings, B. Peng, A. Petrone, T. Henderson, D. Ranasinghe, V. G. Zakrzewski, J. Gao, N. Rega, G. Zheng, W. Liang, M. Hada, M. Ehara, K. Toyota, R. Fukuda, J. Hasegawa, M. Ishida, T. Nakajima, Y. Honda, O. Kitao, H. Nakai, T. Vreven, K. Throssell, J. A. Montgomery Jr., J. E. Peralta, F. Ogliaro, M. J. Bearpark, J. J. Heyd, E. N. Brothers, K. N. Kudin, V. N. Staroverov, T. A. Keith, R. Kobayashi, J. Normand, K. Raghavachari, A. P. Rendell, J. C. Burant, S. S. Iyengar, J. Tomasi, M. Cossi, J. M. Millam, M. Klene, C. Adamo, R. Cammi, J. W. Ochterski, R. L. Martin, K. Morokuma, O. Farkas, J. B. Foresman and D. J. Fox, Gaussian 16, Revision C.01, Gaussian Inc., Wallingford, CT, 2016.

7 a) J. P. Perdew, K. Burke and M. Ernzerhof, *Phys. Rev. Lett.*, 1996, **77**, 3865; b) J. P. Perdew, M. Ernzerhof and K. Burke, *J. Chem. Phys.*, 1996, **105**, 9982; c) M. Ernzerhof and G. E. Scuseria, *J. Chem. Phys.*, 1999, **110**, 5029; d) C. Adamo and V. Barone, *J. Chem. Phys.*, 1999, **110**, 6158.

8 a) M. Dolg, U. Wedig, H. Stoll and H. Preuss, *J. Chem. Phys.*, 1987, **86**, 866; b) A. Bergner, M. Dolg, W. Küchle, H. Stoll and H. Preuss, *Mol. Phys.*, 1993, **80**, 1431; c) G. Igel-Mann, H. Stoll and H. Preuss, *Mol. Phys.*, 1988, **65**, 1321; d) D. Andrae, U. Häussermann, M. Dolg, H. Stoll and H. Preuss, *Theor. Chim. Acta*, 1990, **77**, 123.

9 a) F. Weigend, F. Furche and R. Ahlrichs, *J. Chem. Phys.*, 2003, **119**, 12753; b) F. Weigend and R. Ahlrichs, *Phys. Chem. Chem. Phys.*, 2005, **7**, 3297.

10 S. Grimme, J. Antony, S. Ehrlich and H. Krieg, *J. Chem. Phys.*, 2010, **132**, 154104.

11 T. Lu and F. Chen, *Acta Chim. Sin.*, 2011, **69**, 2393.

12 T. Lu and F. Chen, *J. Comput. Chem.*, 2012, **33**, 580.

13 a) Avogadro: An Open-Source Molecular Builder and Visualization Tool, version 1.2.0, http://avogadro.openmolecules.net/; b) M. D. Hanwell, D. E. Curtis, D. C. Lonie, T. Vandermeersch, E. Zurek and G. R. Hutchison, *J. Cheminf.*, 2012, **4**, 17.

14 a) G. Knizia, http://www.iboview.org; b) G. Knizia, *J. Chem. Theory Comput.*, 2013, **9**, 4834; c) G. Knizia and J. E. M. N. Klein, *Angew. Chem., Int. Ed.*, 2015, **54**, 5518.